RSC Advances

PAPER

View Article Online
View Journal | View Issue

Check for updates

Cite this: *RSC Adv.*, 2018, **8**, 3592

Energy transfer between rare earths in layered rare-earth hydroxides†

Pingping Feng, Xinying Wang, Yushuang Zhao, De-Cai Fang and Xiaojing Yang *

Received 7th November 2017
Accepted 2nd January 2018

DOI: 10.1039/c7ra12206c

rsc.li/rsc-advances

Energy transfer between rare earths in layered rare-earth hydroxides (LRHs) is worth the intensive study because the hydroxyls that act as the bridge connecting the neighbouring rare earths would generate non-radiative transitions. This study focuses on the energy transfer in the intralayer and the adjacent layers of LRHs. A series of $LEu_xTb_{1-x}Hs$ (x = 0, 0.05, 0.2, 0.5, 0.8, and 0.95) was synthesized, the basal spacing (d_{basal}) was adjusted from 8.3 to 46 Å through ion-exchange process, and unilamellar nanosheets were prepared through a delamination process. The luminescence behaviours of the samples demonstrated the following: (1) for the delaminated nanosheets, the quenching effect of both Eu^{3+} and Tb^{3+} was hardly observed. This implies that in the intralayer, the efficiency of energy transfer is extremely low, so that highly-concentrated co-doping does not influence the luminescence and by controlling the Eu/Tb molar ratio, white light can be obtained. (2) For small d_{basal}, *e.g.*, 27 Å, the fluorescence quenching of Tb^{3+} and Eu^{3+} was remarkable, while for large d_{basal}, *e.g.*, 46 Å, the emission of Tb^{3+} emerged and the self-quenching between Eu^{3+} ions weakened. (3) The energy transfer efficiency deceased with an increase in the distance between adjacent layers. In other words, either the energy transfer between Eu^{3+} and Tb^{3+} or the energy migration between Eu^{3+} ions was more efficient when they were located in adjacent layers than in intralayers even when they were the nearest neighbours.

Introduction

Rare earths, owing to their attractive optical properties arising from the 4f electronic shells,[1] play an important role in the development of optical materials. Because of the extremely close radii, it is easy to dope several types of rare earth ions into the same host matrix to realize the tuneable emission colour of luminescence materials.[2] Simultaneously, due to the interaction effects among rare earths,[3] the luminescence intensities of a particular rare earth would be enhanced or quenched with the co-doping of other rare earths.[4] For example, the investigation on energy transfer between Eu^{3+} and Tb^{3+} in $Tb_2(WO_4)_3$:Eu^{3+} indicated that with an increase of the doped Eu^{3+} concentration, the emission of Tb^{3+} became weaker, accompanying the concentration quenching of Eu^{3+}.[5] Such behaviour was also extensively investigated in many other solid phases, such as $TbBO_3$,[6] $NaTbF_4$:Eu,[7] $SrTiO_3$,[8] and $TbPO_4$.[9]

Layered rare earth hydroxides (LRHs), with a general formula of $Ln_2(OH)_{6-m}A_m \cdot nH_2O$ ($0.5 \leq m \leq 2.0$, where Ln stands for trivalent rare earths and A for interlayer anions),[10] are attracting increasing attention since Gándara *et al.* reported their findings in 2006.[11] OH^- groups (and H_2O in some cases of m) coordinate with Ln to form polyhedra and act as the bridge connecting the neighbouring rare earths to form the layer; the layers stack to form the layered structure with interlayer gallery containing A and water. Recently, intercalation, ion exchange, and delamination into 2D crystals have been intensively studied due to LRHs' unique physicochemical properties.[12] LRHs can be also used as an ideal precursor to produce oxide phosphors[13] and the up-conversion host matrix β-$NaYF_4$,[14] bringing new opportunities for LRHs in practical applications. However, only a few studies on energy transfer in LRHs have been reported. Li *et al.*[15] found that for $L(Y_{0.97-x}Tb_{0.03}Eu_x)Hs$ (type m = 1), with an increase of Eu^{3+} concentration, the emission of Tb^{3+} became weaker, suggesting that the energy transferred from Tb^{3+} to Eu^{3+}; the same result was observed in PMMA@SA-LGdH:$Tb_{0.5-x}Eu_x$ (x = 0–0.50).[16] Although it is well known that the coordinated OH^-/H_2O would generate efficient non-radiative emission for the de-excitation of rare earths,[17] this effect of OH^-/H_2O on energy transfer between the rare earths in LRHs has not been studied extensively. Furthermore, this effect and the structural features of LRHs arouse another issue: the energy transfer between the adjacent layers is different from that in the intralayer due to the layered structure.

To clarify these issues, in this study, we synthesized a series of $LEu_xTb_{1-x}Hs$ (x = 0–0.95) and changed the interlayer distances to a large extent. According to the photoluminescence investigation results, we propose a model for the energy transfer in LRHs.

Beijing Key Laboratory of Energy Conversion and Storage Materials, College of Chemistry, Beijing Normal University, Beijing, 100875, China. E-mail: yang.xiaojing@bnu.edu.cn; Fax: +86-10-5880-2075; Tel: +86-10-5880-2960

† Electronic supplementary information (ESI) available: Additional XRD patterns, FT-IR spectra, chemical analysis results, fitting patterns, structure parameters and fluorescence spectra. See DOI: 10.1039/c7ra12206c

Open Access Article. Published on 17 January 2018. Downloaded on 4/8/2026 1:48:07 AM.
This article is licensed under a Creative Commons Attribution-NonCommercial 3.0 Unported Licence.

This journal is © The Royal Society of Chemistry 2018

Open Access Article. Published on 17 January 2018. Downloaded on 4/8/2026 1:48:07 AM.
This article is licensed under a Creative Commons Attribution-NonCommercial 3.0 Unported Licence.

Experimental

Synthesis of $LEu_xTb_{1-x}Hs$ (x = 0, 0.05, 0.2, 0.5, 0.8, and 0.95)

Eu_2O_3 and Tb_4O_7 were obtained from Shanghai Aladdin Biochem Technology Co., Ltd.; sodium dodecyl sulfate (NaDS), from Tianjin Bodi Chemical Co., Ltd; sodium oleate (NaOA), from J&K Scientific Co., Ltd.; and hexamethylenamine (HMT) and the other reagents from Xi Long Chemical Co., Ltd. Eu/Tb nitrate or hydrochloride was prepared from Eu_2O_3/Tb_4O_7 and the corresponding acid by recrystallization.

Different A anion intercalated LRHs are referred as to A-LRHs below. Cl^-- and NO_3^--$LEu_xTb_{1-x}Hs$ (x = 0, 0.05, 0.2, 0.5, 0.8, and 0.95) were prepared through homogenous precipitation method.[18] Briefly, the rare-earth salts were added into an aqueous solution of sodium salt (NaCl or $NaNO_3$) and HMT at the molar ratios of (Eu + Tb) salts/sodium salt/HMT = 1/13/1, and then heated in a Teflon-lined stainless steel autoclave at 90 °C for 12 h. After air-cooling to room temperature, the resultant solid was centrifuged, washed with distilled water and then with anhydrous ethanol several times, and finally dried at 40 °C overnight.

DS^--LRHs were obtained by treating NO_3^--LRHs (0.1 g) in NaDS (0.3708 g, keeping the molar ratio of DS^-/NO_3^- = 3) aqueous solution (80 mL) *via* the DS^-/NO_3^- ion exchange. After autoclaving at 70 °C for 2 days, the resultant solid was collected after filtering. Then, the solid was washed with deionized water and dried at 40 °C for 24 h. In addition, *via* the same method, OA^--LRHs were prepared by mixing 0.1 g NO_3^--LRHs and 1.4982 g NaOA (OA^-/NO_3^- = 12) in 80 mL deionized water and stirring for 24 h.

Synthesis of nanosheets of LRHs

The nanosheets (2D crystals) of the LRHs, noted as NSs-LRHs, were obtained by delamination of the DS^--LRHs samples (0.1 g) in formamide (50 mL)[18] after being heated at 40 °C for 3 days. The nanosheets existed in formamide as a colloidal suspension.

Characterization

Powder X-ray diffraction (XRD) measurement was performed with a Phillips X'Pert Pro MPD diffractometer with Cu-K_α radiation (λ = 0.1541 nm) at room temperature. The generator setting was 40 kV and 40 mA, with a step size of 0.017° and a scan time of 10 s per step. For a Rietveld refinement using the RIETAN-FP software,[19] the XRD patterns were collected at room temperature with step size of 0.017°, scan time of 150 s per step, and 2θ ranging from 4.5° to 120°. At the final refinement, the temperature-factors of H_2O were set to be equal to those of OH^-.

Fourier-transform infrared (FT-IR) spectra were recorded on a Nicolet-380 Fourier-transform infrared spectrometer using the KBr method. Eu and Tb contents were analysed by ICP atomic emission spectroscopy (Jarrell-ASH, ICAP-9000) after the solid samples dissolved in dilute HNO_3 solution, and C, H and N contents were determined by Elementar Vario Elemental analyzer. Atomic force microscope (AFM) observation was carried out in a Veeco NanoScope IIIA microscope after the sample was deposited on a silicon wafer substrate.

Photoluminescence measurements were performed on a Shimadzu RF-5301PC spectrofluorophotometer equipped with a 150 W xenon lamp as the excitation source using monochromator slit widths of 5 nm for NSs-LRHs on both excitation and emission sides and 3 nm for the other samples. The luminescence decay curves were obtained by using Steady State & Time-resolved Fluorescence Spectrometer TemPro-01. All measurements were carried out at room temperature.

Results and discussion

Interlayer spacings and intralayer structure

Fig. 1A depicts the typical XRD patterns of the samples with different interlayer spacings of $LEu_{0.5}Tb_{0.5}H$. The arrangements of the interlayer species are shown in Fig. 1B. The diffraction patterns of the Cl^-- (Fig. 1A(a)) and NO_3^--$LEu_{0.5}Tb_{0.5}H$ (Fig. 1A(b)) samples can be well indexed to orthorhombic (a = 12.874(1), b = 7.299(0), c = 8.439(4) Å) and monoclinic (a = 12.849(0), b = 7.119(1), c = 16.355(0) Å, β = 94.88(1)°) symmetries, respectively, as previously reported,[20] but the two samples have similar basal spacing (d_{basal}) values (8.32 and 8.31 Å, respectively). Larger d_{basal} values are displayed in the samples with different organic anion galleries: ~25 Å for DS^- (Fig. 1A(c)) and ~46 Å for OA^- (Fig. 1A(d)). The latter value was also observed in OA^--LEuH and OA^--LTbH.[21] The d_{basal} values can be construed according to the dimensions and the area per unit charge (S_{charge}) of the layers and the organic ions.[22] S_{charge} values are 0.51 nm^2 for OA^- as calculated using the ChemOffice software,[23] 0.19 nm^2 for DS^-,[18] and 0.23 nm^2 for the layer calculated according to the lattice parameters of Cl^--$LEu_{0.5}Tb_{0.5}H$. The length is ~22 Å for oleate[21] and 18.2 Å for DS^- and the thickness of the layer is 6.5 Å.[18] Thus, for the OA^--LRH samples, the larger $S_{charge}(OA^-)$ value compared to S_{charge} (layer) implies a bilayer arrangement of OA^- anions (Fig. 1B), which is in agreement between the predicted d_{basal} of (2 × 22 + 6.5=) 50.5 Å and the measured value of ~46 Å. For the same reason, the $S_{charge}(DS^-)$

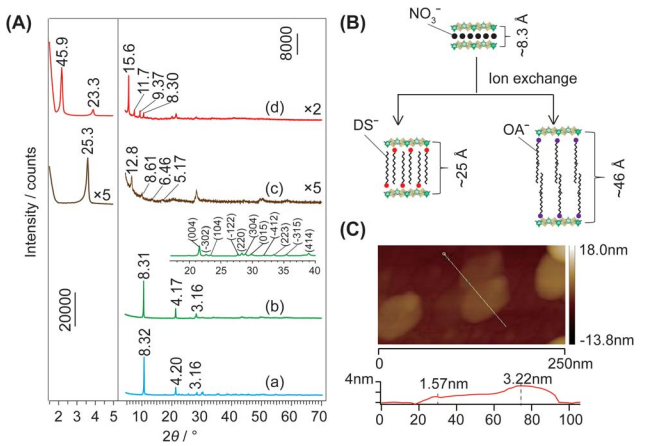

Fig. 1 (A) XRD patterns of (a) Cl^--, (b) NO_3^--, (c) DS^-- and (d) OA^--$LEu_{0.5}Tb_{0.5}H$, (B) the schematic representation of the synthesis processes and the d_{basal} for the samples, and (C) AFM images of NSs-$LEu_{0.5}Tb_{0.5}H$, with the height profiles along the lines in the bottom panel.

Open Access Article. Published on 17 January 2018. Downloaded on 4/8/2026 1:48:07 AM.
This article is licensed under a Creative Commons Attribution-NonCommercial 3.0 Unported Licence.

value are smaller than S_{charge}(layer) value, which allows an alternating antiparallel monolayer arrangement of DS^- (Fig. 1B), which predicts a d_{basal} value of (18.2 + 6.5=) 24.7 Å, agreeing with the observed value of 25.3 Å (Fig. 1A(c)). The thickness of NSs-$LEu_{0.5}Tb_{0.5}H$ was measured as 1.57 nm (Fig. 1C), indicating that the unilamellar were obtained.

Altering x in $LEu_xTb_{1-x}Hs$ invokes barely remarkable d_{basal} changes for the entire Cl^-- or NO_3^--type samples as shown in the XRD patterns (Fig. S1, S2 and Table S1, ESI†). Moreover, the discrepancy of ~0.1 Å, changing irregularly with x, could be explained by the very close natures of Eu^{3+} and Tb^{3+} ions. Conversely, the large difference of ~1.0 Å in d_{basal} for the organic-type samples (Table S1, and Fig. S3, S4, ESI†) indicates the easy deformation of organic interlayer species. The chemical analysis for the Cl^-- (Table S2, ESI†) and NO_3^--LRHs samples (Table S3, ESI†) indicates good agreements between the formulae of $m = 1$ type LRHs (*i.e.* $Ln_2(OH)_5(A^x)_{1/x}\cdot nH_2O$ (ref. 10)) and the analysis results. For all the samples, the interlayer species except for Cl^- are confirmed by the FT-IR spectra (Fig. S5–S7, ESI†). For DS^-- and OA^--$LEu_{0.5}Tb_{0.5}H$, a scanning electron microscopy/energy-dispersive X-ray (SEM/EDX) observation indicated that each element, including Eu, Tb, C, and O (and S for DS^--$LEu_{0.5}Tb_{0.5}H$), was distributed uniformly in the samples (Fig. S8, ESI†).

In $m = 1$ type LRHs, two types of polyhedra, $[Ln(OH)_7(H_2O)]$ and $[Ln(OH)_8(H_2O)]$ (noted as LnO_8 and LnO_9, respectively), should exist. A LnO_8 polyhedron links to two other LnO_8 polyhedra and four LnO_9 polyhedra *via* edge-sharing, forming the host layers.[20a] Eu^{3+} or Tb^{3+} ions in the space group $P2_12_12$ have three Wyckoff sites, which are 2a, 2b and 4c, corresponding to LnO_8, LnO_8 and LnO_9, respectively. In the co-doping case, the smaller ion Tb^{3+} (0.92 Å), rather than Eu^{3+} (0.95 Å),[2] tends to be coordinated in LnO_8,[24] but the radial difference is too small to determine the distribution. As shown in Fig. 2A, three distribution models are proposed to conduct Rietveld refinements for Cl^--$LEu_{0.5}Tb_{0.5}H$ using the analysed composition of $Eu_{0.51}Tb_{0.49}(OH)_{2.45}Cl_{0.42}(CO_3)_{0.06}\cdot 0.87H_2O$ (Table S2, ESI†). The refinement result based on the model of a random distribution (Fig. 2A(a)) is shown in Fig. 3 and Table 1. The calculated pattern is in good agreement with the measured pattern (Fig. 3); the *R*-factors (Table 1), the refined crystal model, and 3D electron density distribution image (Fig. 2B) are satisfactory. However, employing the other two models (Fig. 2A(b) and A(c)) leads to slight differences, including those in *R*-factors (Fig. S9, S10 and Table S4, S5, ESI†). It could be concluded that it is difficult to use the XRD technique to determine which model is preferred because the two rare earths have slight differences in radius and atomic scattering factor.[25] It should be noted that we also combined the fluorescent theoretical calculation to determine the possible distribution of Eu^{3+} and Tb^{3+} in the layers, but in the system, it is difficult for LRHs to be calculated using Gaussian 09 programs.[26] Fig. 4 presents the lattice parameters, calculated by the Rietveld refinements (Fig. S11–S14 and Table S6–S9, ESI†) as a function of Eu^{3+} contents. Both a and b increase linearly with the increase in Eu^{3+} content, thus following Vegard's law.[27] This implies that continuous solid solutions were formed; the same has been reported in LRHs of Y/Eu,[13b,28] Y/Tb[29] and Eu/Gd,[30] which can be explained by the slight distortion energy of the crystal lattice.[29]

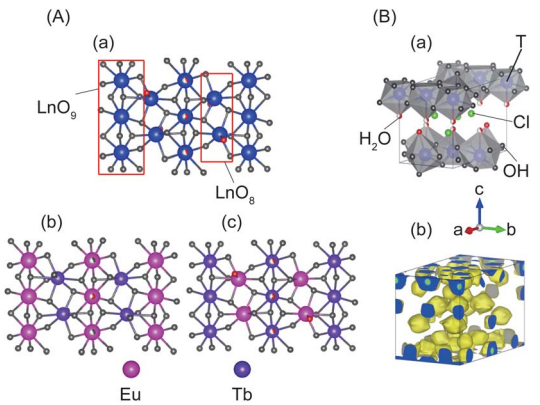

Fig. 2 For Cl^--$LEu_{0.5}Tb_{0.5}H$ with the space group $P2_12_12$, (A) three Eu^{3+}/Tb^{3+} distribution models of the layer projected along [001] directions, (a) random distribution, (b) Tb^{3+} in LnO_8 and Eu^{3+} in LnO_9, (c) Tb^{3+} in LnO_9 and Eu^{3+} in LnO_8; and (B) refined structural models based on the random distribution, (a) crystal structure, (b) 3D electron-density distribution image (isosurface density level of 0.5 $Å^{-3}$). T stands for the rare earth Eu^{3+} or Tb^{3+}.

Photoluminescence of LRHs with different interlayer spacings

The emission and excitation spectra of NO_3^-- and DS^--$LEu_xTb_{1-x}Hs$ are shown in Fig. 5 and S15, ESI.† When $x = 0$, the excitation spectra (Fig. 5a, and S15a, ESI†) monitored with 544 nm emission of Tb^{3+} ($^5D_4 \rightarrow {}^7F_5$) consist of the characteristic f → f transition lines of Tb^{3+} from the $^7F_6$ ground state to the different excited states. Moreover, upon excitation into the $^7F_6 \rightarrow {}^5D_3$ transition of Tb^{3+} at 376 nm, the peaks in the emission spectra (Fig. 5b and S15b, ESI†) can be assigned to the characteristic emission of Tb^{3+}, relating to $^5D_4 \rightarrow {}^7F_j$ ($j = 6, 5, 4, 3$) levels at 489, 544, 584 and 620 nm.[31] However, with Eu^{3+} doping, both NO_3^-- and DS^--LRHs samples primarily exhibit the characteristic emission of Eu^{3+}, corresponding to $^5D_0 \rightarrow {}^7F_{0,1,2,3,4}$ transitions, while the emission of Tb^{3+} is hardly

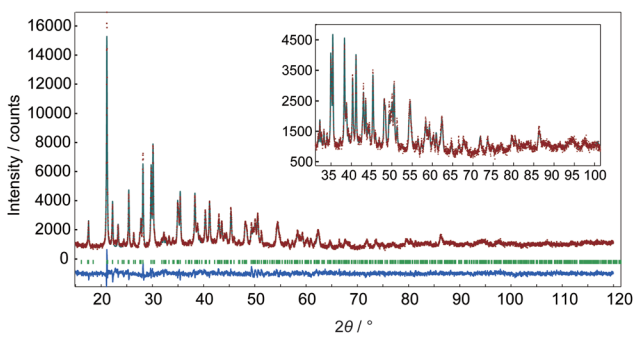

Fig. 3 Fitting patterns of Cl^--$LEu_{0.5}Tb_{0.5}H$. The experimental and simulated intensities are plotted as dotted and solid lines, respectively; the line at the bottom is their intensity difference, the tick marks indicate the positions of all possible Bragg reflections from the structure model.

This journal is © The Royal Society of Chemistry 2018

Open Access Article. Published on 17 January 2018. Downloaded on 4/8/2026 1:48:07 AM.
This article is licensed under a Creative Commons Attribution-NonCommercial 3.0 Unported Licence.

Table 1 Structure parameters of Cl^--$LEu_{0.5}Tb_{0.5}H$[a]

Species	Wyckoff index	x	y	z	g	B/Å^2
T1	4c	0.271(5)	0.248(8)	0.929(9)	1.0	0.841(4)
T2	2b	0	0.5	0.949(3)	1.0	0.841(4)
T3	2a	0	0	0.930(5)	1.0	0.841(4)
OH(1)	4c	0.485(9)	0.270(2)	0.906(6)	1.0	0.303(0)
OH(2)	4c	0.083(0)	0.229(2)	0.838(1)	1.0	0.303(0)
OH(3)	4c	0.160(8)	0.411(9)	0.085(9)	1.0	0.303(0)
OH(4)	4c	0.646(3)	0.449(8)	0.925(7)	1.0	0.303(0)
OH(5)	4c	0.143(7)	0.775(5)	0.828(5)	1.0	0.303(0)
H_2O(1)	4c	0.198(1)	0.827(2)	0.378(3)	1.0	2.922(5)
H_2O(2)	2b	0	0.5	0.608(5)	0.36	2.922(5)
H_2O(3)	2a	0	0	0.629(0)	0.54	2.922(5)
Cl	4c	0.125(6)	0.216(9)	0.430(9)	1.0	2.723(7)

[a] Space group: $P2_12_12$ (no. 18); a = 12.874(0) Å; b = 7.299(2) Å; c = 8.439(3) Å; V = 793.0(4) Å^3; R_{wp} = 7.329%, R_p = 5.726%, R_R = 19.458%, R_e = 2.834%, S = 2.5864%. T stands for the rare earth Eu^{3+} or Tb^{3+}, g stands for the occupancy, B stands for the temperature-factor.

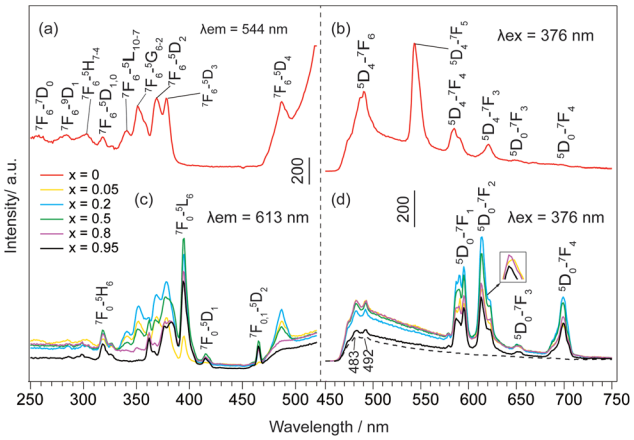

Fig. 5 (a, c) Excitation and (b, d) emission spectra of NO_3^--LEu_x-$Tb_{1-x}Hs$. The peaks at 483 and 492 nm (dashed line) are due to spectral responses of the equipment by the blank.

observed (Fig. 5d and S15d, ESI†). The presence of the excitation bands of Tb^{3+} in the excitation spectra (Fig. 5c and S15c, ESI†) when monitored at 613 nm with $^5D_0 \rightarrow {}^7F_2$ of Eu^{3+} indicates that an efficient energy transfer occurred from Tb^{3+} to Eu^{3+} in these samples,[32] also suggesting that Eu^{3+} had been successfully doped into the LTbH lattice. When $x < 0.5$, the luminescence intensity of Eu^{3+} increases with the increasing Eu^{3+} concentration; however, when $x \geq 0.5$, it becomes weaker and weaker. This result suggests that the luminescence of Eu^{3+} is a competitive result of a dual effect: (1) the increase of Eu^{3+} concentration enhances the probability of energy transfer from Tb^{3+} to Eu^{3+} and (2) it also increases the probability of nonradioactive energy migration between Eu^{3+} ions to quenching centres, where the excitation energy is lost nonradiatively.[33]

For OA^--$LEu_xTb_{1-x}Hs$ with larger d_{basal}, the luminescence behaviour changes greatly as compared to that of NO_3^- and DS^--$LEu_xTb_{1-x}Hs$. In the excitation spectra monitored at 544 nm (Fig. 6A(a)), no matter whether Eu^{3+} is doped, the peaks attributed to the intra-4f^8 transitions from $^7F_6$ to $^5L_{10-7}$, $^5G_{6-2}$, and $^5D_{2,3}$ states of Tb^{3+} are observable; as monitored with Eu^{3+} emission (Fig. 6A(b)), the excitation bands of Tb^{3+} still exist. Under 376 nm excitation, the characteristic emission of Tb^{3+} emerges noticeably. The luminescence intensity of Tb^{3+} decreases with increasing x from 0 to 0.95 and the intensity for Tb^{3+} at $x = 0.05$ is slightly lower than that at $x = 0$. When $x < 0.8$, the luminescence intensity of Eu^{3+} increases gradually with the increasing Eu^{3+} concentration; when $x \geq 0.8$, it wears off (Fig. 6A(c)).

Overall, under the same measurement condition, the quenching of Tb^{3+} weakens with the increase in d_{basal}, and the quenching concentration of Eu^{3+} observable at $x = 0.5$ for NO_3^-- and DS^--$LEu_xTb_{1-x}Hs$ and at $x = 0.8$ for OA^--$LEu_xTb_{1-x}Hs$ demonstrates that the expansion extent of the interlayer distances plays a decisive role in the energy transfer. Such energy transfers are realized primarily between the adjacent layers rather than in the intralayer, where the rare earths are even closer.

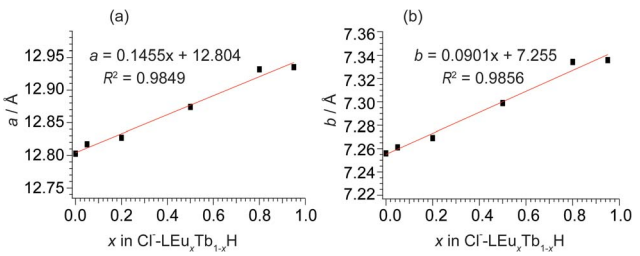

Fig. 4 The correlation of lattice parameters of (a) a and (b) b with the Eu^{3+} content in Cl^--$LEu_xTb_{1-x}Hs$.

Photoluminescence of 2D crystals

In the case of exfoliated 2D crystals, an infinite interlayer distance or only the energy transfer in the intralayer could be reasonably considered. Under excitation at 376 nm, the emission spectra (Fig. 6B(c)) of NSs-LRHs show both luminescence intensities of Eu^{3+} and Tb^{3+} in proportion to their own concentrations. Furthermore, as monitored at λ_{em} = 613 nm, the very weak bands in the excitation spectra (Fig. 6B(b)) imply that only a small amount of energy was transferred from Tb^{3+} to Eu^{3+}. This behaviour reveals that the energy transfer between the neighbouring rare earths in the intralayer could be negligible. This result is in agreement with the observations in the layered compounds discussed above.

Fig. 7 shows the Commission International de L'Eclairage (CIE) chromaticity coordinates for NSs-LRHs excited at 284 and 318 nm. The related emission spectra are shown in Fig. S16, ESI.† The (x, y) coordinates vary systematically from green to red with the doped concentration of Eu^{3+}, manifesting that the as-obtained NSs-$LEu_xTb_{1-x}Hs$ can show multicolour emissions in the visible region when excited by the selective excitation bands. It should be noted that the colour coordinate (0.3552, 0.3562) of $x = 0.8$ samples excited under 284 nm results in white light emission. It is inevitable to obtain the white light emission in the Eu^{3+} and Tb^{3+} co-doping 2D crystals because the energy transfer in the intralayer is negligible.

Open Access Article. Published on 17 January 2018. Downloaded on 4/8/2026 1:48:07 AM.
This article is licensed under a Creative Commons Attribution-NonCommercial 3.0 Unported Licence.

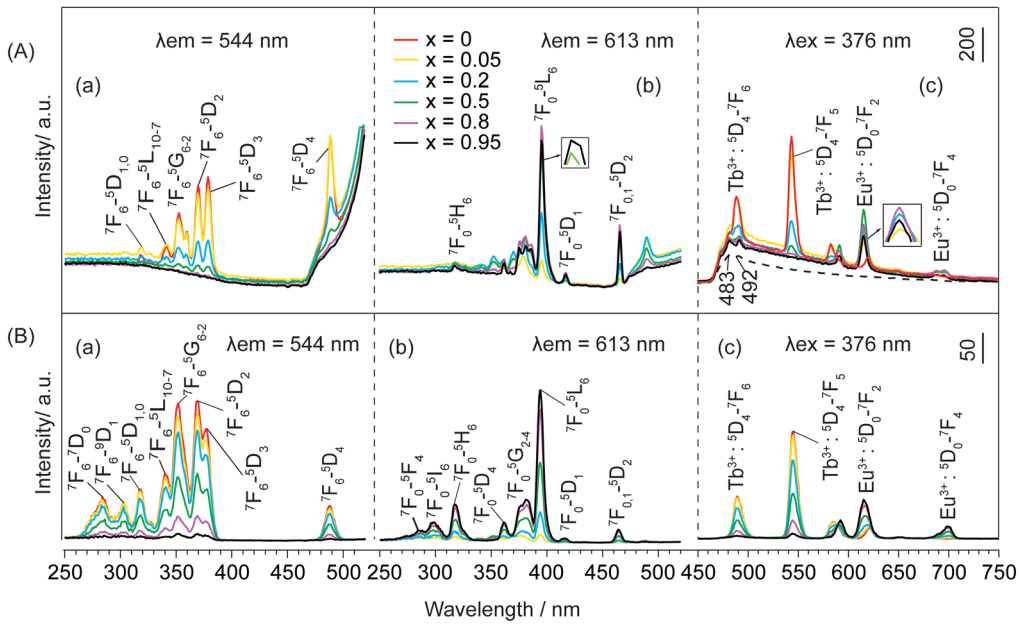

Fig. 6 Excitation spectra monitored at (a) 544 nm, (b) 613 nm and emission spectra excited at (c) 376 nm of (A) OA^{-}- $LEu_xTb_{1-x}Hs$ (the peaks at 483 and 492 nm of the dashed line are due to spectral responses of the equipment by the blank) and (B) NSs-$LEu_xTb_{1-x}Hs$.

Luminescence lifetimes

Two possible routes of energy transfer between Eu^{3+} and Tb^{3+} in LRHs are proposed in Scheme 1. Route (I), as shown in Scheme 1, represents that energy is transferred through the OH group, which bridges adjacent Eu^{3+} and Tb^{3+} located in the intralayer. The OH groups de-excite the energy transferred from Tb^{3+}, making the transfer inefficient. In route (II), the energy is directly transferred from Tb^{3+} to Eu^{3+} as the two ions reside in the adjacent layers. The results discussed above indicate that the transfer would be more efficient through route (II) than route (I). In other words, route (II) might be the main procedure of energy transfer in LRHs. To further clarify this, we investigated the luminescence lifetimes for LTbH ($x = 0$) and $LEu_{0.05}Tb_{0.95}H$ ($x = 0.05$). The luminescence decay curves of Tb^{3+} are depicted in Fig. 8.

As shown in Fig. 8, the curves can be fitted into a double-exponential function according to eqn (1),

$$I(t) = I_0 + A_1 \exp(-t/\tau_1) + A_2 \exp(-t/\tau_2) \quad (1)$$

where I and I_0 are the phosphorescence intensities; A_1 and A_2, constants; t, decay time (ms); and τ_1 and τ_2, the decay times (ms) for the exponential components, respectively.[34] The efficiency of energy transfer (η_{ET}) from the donor Tb^{3+} to the acceptor Eu^{3+} could be calculated using eqn (2),

$$\eta_{ET} = 1 - \tau/\tau_0 \quad (2)$$

where τ and τ_0 are the luminescence lifetimes of Tb^{3+} for the doped and undoped samples at the same donor concentration.[35] The calculated τ and η_{ET} are listed in Table 2. The η_{ET} reaches 98.1% for NO_3^{-}-$LEu_{0.05}Tb_{0.95}H$ and 95.0% for DS^{-}-$LEu_{0.05}Tb_{0.95}H$; we ignored the minor change in the Tb^{3+} concentration. The luminescence lifetimes of Tb^{3+} ($^5D_4$) are

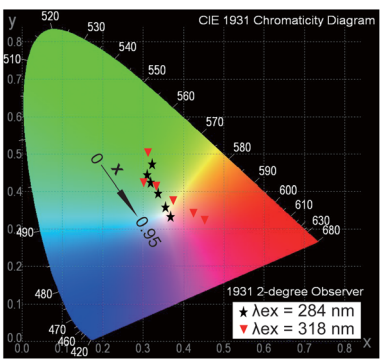

Fig. 7 CIE chromaticity coordinates for NSs-$LEu_xTb_{1-x}Hs$ excited at 284 and 318 nm.

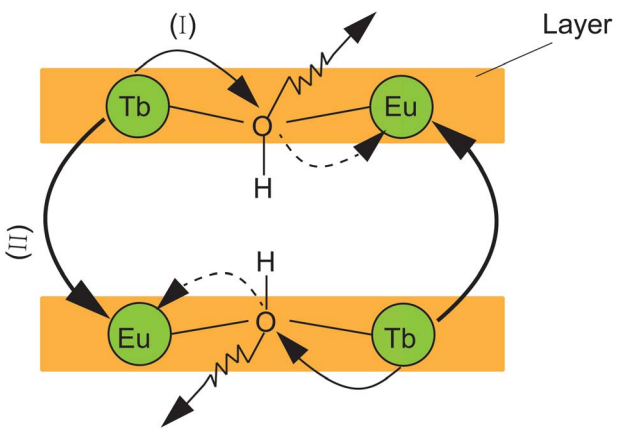

Scheme 1 Illustration of energy transfer between Eu^{3+} and Tb^{3+} in LRHs.

This journal is © The Royal Society of Chemistry 2018

Open Access Article. Published on 17 January 2018. Downloaded on 4/8/2026 1:48:07 AM.
This article is licensed under a Creative Commons Attribution-NonCommercial 3.0 Unported Licence.

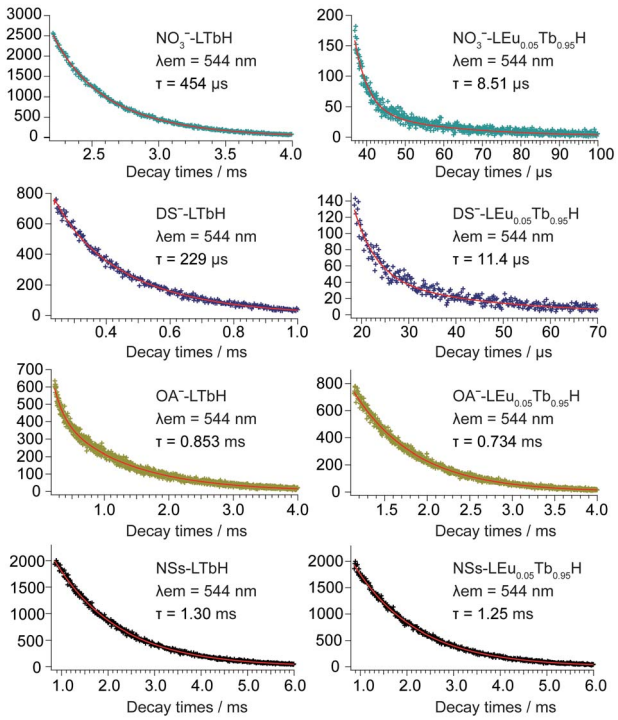

Fig. 8 Luminescence decay curves of LTbH and $LEu_{0.05}Tb_{0.95}H$ monitored at 544 nm, corresponding to $^5D_4$–$^7F_5$ level of Tb^{3+}.

Table 2 The lifetimes τ for Tb^{3+} and energy transfer efficiency (η_{ET}) when $x = 0$ and 0.05 upon excitation with 374 nm

x	NO_3^- (μs)	DS^- (μs)	OA^- (ms)	NSs (ms)
0	454	229	0.853	1.30
0.05	8.51	11.4	0.734	1.25
η_{ET} (%)	98.1	95.0	14.0	3.85

generally observed in the range of milliseconds because of the forbidden nature of the f–f transition,[36] but in the present case, the lifetimes of NO_3^--, OA^-- and NSs-$LEu_{0.05}Tb_{0.95}H$ change from microsecond to millisecond, corresponding to the increase of d_{basal}. This indicates that the small interlayer distance has high η_{ET}. The lifetime of OA^--$LEu_{0.05}Tb_{0.95}H$ is very close to that of OA^-LTbHs, denoting that its η_{ET} becomes extremely insignificant. Such a result is observable in the case of the 2D crystals of NSs-LRHs (Table 2). Since the energy transfer probability from Tb^{3+} to Eu^{3+} is proportional to R^{-6}, where R is the average distance between the ions,[37] the expansion of the interlayer distance and even delamination, leading to the increase of R, lower the energy transfer efficiency.

The above results support strongly that the energy transfer between Eu^{3+} and Tb^{3+} in route (II), as illustrated in Scheme 1, is predominant in LRHs.

Conclusions

Due to the unique structure of LRHs, the de-excitation of OH groups on the energy transfer between rare earths is effective in the intralayer. This leads to the fact that the efficiency of the energy transfer from Tb^{3+}/Eu^{3+} to Eu^{3+} in the intralayer is very weak, and efficient energy transfer is primarily achieved when the rare earths locate in adjacent layers. White light can be obtained in the 2D crystals of $LEu_{0.8}Tb_{0.2}H$ under 284 nm. This might be of potential use as a natural white light source under ultraviolet light excitation.

Conflicts of interest

There are no conflicts to declare.

Acknowledgements

This study was supported by the National Science Foundation of China (Grants. 51572031 and 51272030) and Program for Changjiang Scholars and Innovative Research Team in University.

Notes and references

1 A. Gupta, N. Brahme and D. P. Bisen, *J. Lumin.*, 2014, **155**, 112.
2 H. Shen, S. Feng, Y. Wang, Y. Gu, J. Zhou, H. Yang, G. Feng, L. Li, W. Wang, X. Liu and D. Xu, *J. Alloys Compd.*, 2013, **550**, 531.
3 L. G. V. Uitert and S. Iida, *J. Chem. Phys.*, 1962, **37**, 986.
4 E. Nakazawa and S. Shionoya, *J. Chem. Phys.*, 1967, **47**, 3211.
5 Z. Hou, Z. Cheng, G. Li, W. Wang, C. Peng, C. Li, P. a. Ma, D. Yang, X. Kang and J. Lin, *Nanoscale*, 2011, **3**, 1568.
6 J. Yang, C. Zhang, C. Li, Y. Yu and J. Lin, *Inorg. Chem.*, 2008, **47**, 7262.
7 Z. Chen, Z. Geng, D. Shao, Z. Zhou and Z. Wang, *CrystEngComm*, 2012, **14**, 2251.
8 G. García-Rosales, F. Mercier-Bion, R. Drot, G. Lagarde, J. Roques and E. Simoni, *J. Lumin.*, 2012, **132**, 1299.
9 W. Di, X. Wang, P. Zhu and B. Chen, *J. Solid State Chem.*, 2007, **180**, 467.
10 K.-H. Lee and S.-H. Byeon, *Eur. J. Inorg. Chem.*, 2009, **2009**, 4727.
11 F. Gándara, J. Perles, N. Snejko, M. Iglesias, B. Gómez-Lor, E. Gutiérrez-Puebla and M. Á. Monge, *Angew. Chem., Int. Ed.*, 2006, **45**, 7998.
12 X. Wu, J.-G. Li, Q. Zhu, W. Liu, J. Li, X. Li, X. Sun and Y. Sakka, *J. Mater. Chem. C*, 2015, **3**, 3428.
13 (*a*) K.-H. Lee, B.-I. Lee, J.-H. You and S.-H. Byeon, *Chem. Commun.*, 2010, **46**, 1461; (*b*) Q. Zhu, J.-G. Li, C. Zhi, X. Li, X. Sun, Y. Sakka, D. Golberg and Y. Bando, *Chem. Mater.*, 2010, **22**, 4204.
14 (*a*) B. Shao, Q. Zhao, Y. Jia, W. Lv, M. Jiao, W. Lu and H. You, *Chem. Commun.*, 2014, **50**, 12706; (*b*) B. Shao, Q. Zhao, W. Lv, M. Jiao, W. Lu and H. You, *J. Mater. Chem. C*, 2015, **3**, 1091.
15 X. Wu, J.-G. Li, J. Li, Q. Zhu, X. Li, X. Sun and Y. Sakka, *Sci. Technol. Adv. Mater.*, 2013, **14**, 015006.
16 L. Liu, M. Yu, J. Zhang, B. Wang, W. Liu and Y. Tang, *J. Mater. Chem. C*, 2015, **3**, 2326.

Open Access Article. Published on 17 January 2018. Downloaded on 4/8/2026 1:48:07 AM.
This article is licensed under a Creative Commons Attribution-NonCommercial 3.0 Unported Licence.

17 R. M. Supkowski and W. D. Horrocks Jr, *Inorg. Chim. Acta*, 2002, **340**, 44.
18 Y. Zhao, J.-G. Li, M. Guo and X. Yang, *J. Mater. Chem. C*, 2013, **1**, 3584.
19 F. Izumi and K. Momma, *Solid State Phenom.*, 2007, **130**, 15.
20 (*a*) F. Geng, Y. Matsushita, R. Ma, H. Xin, M. Tanaka, F. Izumi, N. Iyi and T. Sasaki, *J. Am. Chem. Soc.*, 2008, **130**, 16344; (*b*) F. Geng, Y. Matsushita, R. Ma, H. Xin, M. Tanaka, N. Iyi and T. Sasaki, *Inorg. Chem.*, 2009, **48**, 6724.
21 B.-I. Lee, J.-S. Bae, E.-S. Lee and S.-H. Byeon, *Bull. Korean Chem. Soc.*, 2012, **33**, 601.
22 G. Huang, S. Ma, X. Zhao, X. Yang and K. Ooi, *Chem. Mater.*, 2010, **22**, 1870.
23 http://www.cambridgesoft.com/.
24 L. Hu, R. Ma, T. C. Ozawa and T. Sasaki, *Inorg. Chem.*, 2010, **49**, 2960.
25 D. T. Cromer, A. C. Larson and J. T. Waber, *Acta Crystallogr.*, 1964, **17**, 1044.
26 M. J. Frisch, G. W. Trucks, H. B. Schlegel, G. E. Scuseria, M. A. Robb, J. R. Cheeseman, G. Scalmani, V. Barone, B. Mennucci, G. A. Petersson, H. Nakatsuji, M. Caricato, X. Li, H. P. Hratchian, A. F. Izmaylov, J. Bloino, G. Zheng, J. L. Sonnenberg, M. Hada, M. Ehara, K. Toyota, R. Fukuda, J. Hasegawa, M. Ishida, T. Nakajima, Y. Honda, O. Kitao, H. Nakai, T. Vreven, J. A. Montgomery Jr, J. E. Peralta, F. Ogliaro, M. Bearpark, J. J. Heyd, E. Brothers, K. N. Kudin, V. N. Staroverov, R. Kobayashi, J. Normand, K. Raghavachari, A. Rendell, J. C. Burant, S. S. Iyengar, J. Tomasi, M. Cossi, N. Rega, J. M. Millam, M. Klene, J. E. Knox, J. B. Cross, V. Bakken, C. Adamo, J. Jaramillo, R. Gomperts, R. E. Stratmann, O. Yazyev, A. J. Austin, R. Cammi, C. Pomelli, J. W. Ochterski, R. L. Martin, K. Morokuma, V. G. Zakrzewski, G. A. Voth, P. Salvador, J. J. Dannenberg, S. Dapprich, A. D. Daniels, O. Farkas, J. B. Foresman, J. V. Ortiz, J. Cioslowski and D. J. Fox, *GAUSSIAN 09 (Revision A.02)*, Gaussian, Inc., Wallingford, CT, 2009.
27 Q. Yuan, Q. Liu, W.-G. Song, W. Feng, W.-L. Pu, L.-D. Sun, Y.-W. Zhang and C.-H. Yan, *J. Am. Chem. Soc.*, 2007, **129**, 6698.
28 L. Wang, D. Yan, S. Qin, S. Li, J. Lu, D. G. Evans and X. Duan, *Dalton Trans.*, 2011, **40**, 11781.
29 J. Liang, R. Ma and T. Sasaki, *Dalton Trans.*, 2014, **43**, 10355.
30 Z. Xu, C. Li, G. Li, R. Chai, C. Peng, D. Yang and J. Lin, *J. Phys. Chem. C*, 2010, **114**, 2573.
31 A. Huignard, T. Gacoin and J.-P. Boilot, *Chem. Mater.*, 2000, **12**, 1090.
32 J. Yang, G. Li, C. Peng, C. Li, C. Zhang, Y. Fan, Z. Xu, Z. Cheng and J. Lin, *J. Solid State Chem.*, 2010, **183**, 451.
33 L. Zhou, J. Yang, S. Hu, Y. Luo and J. Yang, *J. Mater. Sci.*, 2015, **50**, 4503.
34 M. Back, M. Boffelli, A. Massari, R. Marin, F. Enrichi and P. Riello, *J. Nanopart. Res.*, 2013, **15**, 1–14.
35 Y.-C. Li, Y.-H. Chang, Y.-S. Chang, Y.-J. Lin and C.-H. Laing, *J. Phys. Chem. C*, 2007, **111**, 10682.
36 R. Chai, H. Lian, C. Li, Z. Cheng, Z. Hou, S. Huang and J. Lin, *J. Phys. Chem. C*, 2009, **113**, 8070.
37 K. Riwotzki, H. Meyssamy, A. Kornowski and M. Haase, *J. Phys. Chem. B*, 2000, **104**, 2824.

This journal is © The Royal Society of Chemistry 2018